QUANTUM NOISE AND MUTIPLE ANDREEV REFLECTIONS IN SUPERCONDUCTING CONTACTS

A. MARTíN-RODERO, J. C. CUEVAS* AND A. LEVY YEYATI
Departamento de Física Teórica de la Materia Condensada Universidad Autónoma de Madrid, E-28049 Madrid, Spain

AND

R. CRON, M.F. GOFFMAN, D. ESTEVE AND C. URBINA
Service de Physique de l'Etat Condensé, Commissariat à u'Energie Atomique, Saclay, F-91191 Gif-sur-Yvette Cedex, France

Abstract. The mechanism of multiple Andreev reflections (MAR) leads to a rather complex behavior of the noise spectral density in superconducting quantum point contacts as function of the relevant parameters. In this contribution we analyze recent theoretical and experimental efforts which have permitted to clarify this issue to a great extent. The theoretical description of noise in the coherent MAR regime will be summarized, discussing its main predictions for equilibrium and non-equilibrium current fluctuations. We then analyze noise measurements in well characterized superconducting atomic contacts. These systems allow for a direct test of the theoretical predictions without fitting parameters. In particular, the increase of the effective charge corresponding to the openning of higher order Andreev channels has been verified.

1. Introduction

Non-equilibrium current fluctuations provide a powerful probe of the transport mechanisms in mesoscopic structures. Indeed, in contrast to the universal equilibrium *thermal noise*, even the low-frequency power spectrum of these nonequilibrium fluctuations, or "shot-noise", contains a wealth of information on the interactions and quantum correlations between electrons [1]. When the current I is made up from independent shots, the low fre-

quency spectrum acquires the well-known Poissonian form $S = 2qI$, where q is the "effective charge" transferred at each shot. This result was derived by Schottky as early as in 1918 for a vacuum diode [2]. In the case of normal, i.e. nonsuperconducting, metallic reservoirs, the charge of the shots is simply the electron charge e. Interactions and correlations lead to large deviations from this value. One of the most striking examples is the fractional charge of quasiparticles in the fractional quantum Hall regime, as it was evidenced through noise measurements [3]. The mechanism giving rise to superconductivity is another source of correlations among electrons. How big are the shots when superconducting electrodes are involved? And more generally, what can we learn from the analysis of noise in superconducting nanostructures? These are the central questions that we shall address in this contribution.

Noise phenomena when superconductors are involved is of particular interest due to the peculiar nature of the charge transfer mechanisms arising from the presence of a Cooper pair condensate. Thus, for instance, the current between a superconducting reservoir and a normal one connected by a short normal wire proceeds through the process of Andreev reflection in which charge is transferred in shots of $2e$, thus resulting in a doubling of the noise with respect to the normal case [4]. When two superconducting electrodes connected through structures such as tunnel junctions or short weak links are voltage biased on an energy scale eV smaller than the superconducting gap Δ, the current proceeds through multiple Andreev reflections (MAR) [5]. Fig. 1 illustrates the lowest order processes contributing to quasiparticle transport in a superconducting junction. In a n-order MAR process, which has a threshold voltage of $eV = 2\Delta/n$, an electron (or hole) is created on the right (left) electrode after $n-1$ Andreev reflections, the total charge transmitted in the whole process being ne. For a given voltage many such processes can contribute to the current, but roughly speaking, "giant" shots, with an effective charge $q \sim e(1 + 2\Delta/eV)$ are expected at subgap energies. Of course, the exact value of q, like all other transport properties of a coherent nanostructure, depends on its "mesoscopic pin code", i.e. the set of transmission coefficients τ_i characterizing its conduction channels.

Although the MAR mechanism in superconducting junctions was first introduced nearly two decades ago [5], a complete understanding of transport in the coherent MAR regime has only recently been achieved due to the combination of theoretical and experimental developments. On the theoretical side, fully quantum mechanical calculations have allowed to obtain detailed quantitative predictions for different transport properties [6, 7, 8, 9, 11, 10, 12, 13].

At the same time, the development of atomic size contacts by means

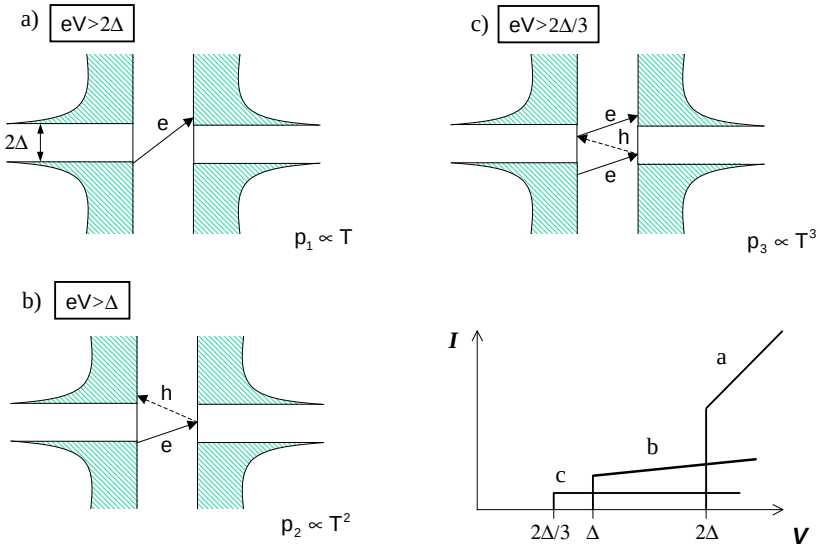

Figure 1. Schematic representation of the MAR processes. We have represented the density of states of both electrodes. The transmission probability is τ. In the upper panel we describe the single-quasiparticle process in which an electron tunnels through the system overcoming the superconducting gap due to a voltage $eV \geq 2\Delta$. The intermediate panel shows an Andreev reflection in which an electron is reflected as a hole, which can reach an empty state in the left electrode if the voltage is $eV \geq \Delta$. During this process, which for small transmission has a probability τ^2, two electron charges are transferred as a Cooper pair from left to right. The lower panes shows an Andreev reflection of order 3 in which an Andreev reflected hole is still Andreev reflected as an electron, which finally reaches an empty state in the right electrode. In this process, whose threshold voltage is $eV = 2\Delta/3$, three charges are transferred with a probablity τ^3.

of break junction and STM techniques [14, 15, 16, 17, 18, 19, 20, 21], has opened the possibility of a direct comparison between theory and experiments [17, 18, 19, 20, 21]. These systems are caracterised by a few conduction channels whose transmission coefficients can be determined experimentally with great accuracy [17, 18, 19].

In the present paper we shall review recent advances in the understanding of noise phenomena in nano-scale superconducting devices. In the first section we summarize the theoretical description of noise in the coherent MAR regime. An approach based on non-equilibrium Green functions techniques will be discussed with some detail. We then present the main theoretical predictions for equilibrium and non-equlibrium current fluctuations. The experimental studies of noise in SNS nanostructures are reviewed in Sect. III. We shall mainly concentrate in the discussion of noise measurements using well characterized superconducting atomic contacts. Finally, in Sect. IV we present our concluding remarks.

2. Theoretical description of noise in the coherent MAR regime

The MAR mechanism was introduced by Klapwijk *et al.* [5] to explain the subgap structure observed in different types of superconducting junctions. That first approach was based on semi-classical arguments which neglected quantum interference between different processes. An earlier microscopic theory due to Schrieffer and Wilkins [22] attempted to introduce the contribution of multiparticle processes like the ones depicted in Fig. 1 by means of lowest order perturbation theory in the tunnel Hamiltonian coupling two superconducting leads. In spite of being a fully quantum mechanical approach, this Multiparticle Tunneling Theory (MPT), is plagued with divergencies which can only be avoided by carrying out the calculation up to infinite order. This goal was achieved more recenlty by the so called Hamiltonian approach [9], based on a Green functions formalism, which demonstrated the essential equivalence of the MPT and MAR arguments.

Recent calculations in the coherent MAR regime have been based on two different approaches: the Hamiltonian approach mentioned above and the scattering approach developed in Refs. [7] and [8]. Although both approaches yield equivalent results in the limit when the energy dependence of the normal transmission can be neglected, each one has its own advantages. Thus, although the scattering approach might appear as conceptualy simpler, the Hamiltonian approach is more rigorous as it does not rely on ad-hoc assumptions on boundary conditions. In addition the use of Green function techniques allows to deal, for instance, with electron correlation effects within this approach. In what follows we briefly sketch the basic ingredients in the Hamiltonian approach for the description of a voltage biased superconducting contact. We shall consider the case of a superconducting quantum point-contact, i.e. a short ($L \ll \xi_0$) mesoscopic constriction between two superconducting electrodes with a constant applied bias voltage V. For the range $eV \sim \Delta$ one can neglect the energy dependence of the transmission coefficients and all transport properties can be expressed as a superposition of independent channel contributions. Thus, we will concentrate in analyzing a single channel model which can be described by the following Hamiltonian [9]

$$\hat{H}(t) = \hat{H}_L + \hat{H}_R + \sum_{\sigma} \left(v e^{i\phi(t)/2} c^{\dagger}_{L\sigma} c_{R\sigma} + \ h.c. \ \right), \tag{1}$$

where $\hat{H}_{L,R}$ are the BCS Hamiltonians for the left and right uncoupled electrodes, $\phi(t) = \phi_0 + 2eVt/\hbar$ is the time-dependent superconducting phase difference, which after a gauge transformation enters as a phase factor in the hopping terms describing electron transfer between both electrodes. To obtain the transport properties we use a perturbative Green functions

approach including processes up to infinite order in the hopping parameter v (all MAR processes of arbitrary order are in this way naturally included). In the normal state, the one-channel contact is characterized by its transmission coefficient τ, which as a function of v adopts the form $\tau = 4(v/W)^2/(1+(v/W)^2)^2$, where $W = 1/\pi\rho_F$, ρ_F being the electrodes density of states at the Femi energy [9]. Within this model the current operator is given by

$$\hat{I}(t) = \frac{ie}{\hbar}\sum_{\sigma}\left[ve^{i\phi(t)/2}c^{\dagger}_{L\sigma}(t)c_{R\sigma}(t) - v^{*}e^{-i\phi(t)/2}c^{\dagger}_{R\sigma}(t)c_{L\sigma}(t)\right]. \qquad (2)$$

The current noise spectral density is defined as

$$\begin{aligned} S(\omega,t) &= \hbar\int dt'\ e^{i\omega t'}\langle\delta\hat{I}(t+t')\delta\hat{I}(t) + \delta\hat{I}(t)\delta\hat{I}(t+t')\rangle \\ &\equiv \hbar\int dt'\ e^{i\omega t'}\ K(t,t'), \end{aligned} \qquad (3)$$

where $\delta\hat{I}(t) = \hat{I}(t) - \langle\hat{I}(t)\rangle$ is the time-dependent fluctuations in the current.

The relevant quantities to be determined can be expressed in terms of non-equilibrium Keldysh Green functions [23] in a Nambu representation $\hat{G}^{+-}_{ij}(t,t')$ and $\hat{G}^{-+}_{ij}(t,t')$ where $i,j \equiv L,R$ defined as

$$\hat{G}^{+-}_{i,j}(t,t') = i\begin{pmatrix} \langle c^{\dagger}_{j\uparrow}(t')c_{i\uparrow}(t)\rangle & \langle c_{j\downarrow}(t')c_{i\uparrow}(t)\rangle \\ \langle c^{\dagger}_{j\uparrow}(t')c^{\dagger}_{i\downarrow}(t)\rangle & \langle c_{j\downarrow}(t')c^{\dagger}_{i\downarrow}(t)\rangle \end{pmatrix}, \qquad (4)$$

and obey the relation $\hat{G}^{-+}_{i,j}(t,t') = -\hat{\sigma}_x\left[\hat{G}^{+-}_{j,i}(t',t)\right]^{T}\hat{\sigma}_x$, $\hat{\sigma}_x$ being the Pauli matrix.

Then, the mean current and the kernel $K(t,t')$ in the noise spectral density are given by

$$\begin{aligned} <\hat{I}(t)> &= \frac{e}{\hbar}\ \mathrm{Tr}\left[\hat{\sigma}_z\left(\hat{v}(t)\hat{G}^{+-}_{RL}(t,t) - \hat{v}^{\dagger}(t)\hat{G}^{+-}_{LR}(t,t)\right)\right] \\ K(t,t') &= \frac{2e^2}{\hbar^2}\Big\{\mathrm{Tr}\left[\hat{\sigma}_z\hat{v}^{\dagger}(t)\hat{G}^{+,-}_{LL}(t,t')\hat{\sigma}_z\hat{v}(t')\hat{G}^{-,+}_{RR}(t',t) - \right. \\ &\left.\hat{\sigma}_z\hat{v}^{\dagger}(t)\hat{G}^{+,-}_{LR}(t,t')\hat{\sigma}_z\hat{v}^{\dagger}(t')\hat{G}^{-,+}_{LR}(t',t)\right] + (t\to t')\Big\}, \end{aligned} \qquad (5)$$

where $\hat{\sigma}_z$ is the Pauli matrix, Tr denotes the trace in the Nambu space and $\hat{v}$ is the hopping in this representation

$$\hat{v}(t) = \begin{pmatrix} ve^{i\phi(t)/2} & 0 \\ 0 & -v^{*}e^{-i\phi(t)/2} \end{pmatrix}. \qquad (6)$$

The expression of the Kernel in terms of one-particle Green functions (Eq. 5) has been obtained using Wick's theorem. This is equivalent to neglect correlations beyond the BCS mean-field theory. As mentioned above, in order to determine the Green functions we follow a perturbative scheme and treat the coupling term in Hamiltonian (1) as a perturbation. The unperturbed Green functions, $\hat{g}$, correspond to the uncoupled electrodes in equilibrium. Thus, the retarded and advanced components adopt the BCS form: $\hat{g}^{r,a}(\epsilon) = g^{r,a}(\epsilon)\hat{1} + f^{r,a}(\epsilon)\hat{\sigma}_x$, where $g^{r,a}(\epsilon) = -(\epsilon^{r,a}/\Delta)f(\epsilon) = -\epsilon^{r,a}/W\sqrt{\Delta^2 - (\epsilon^{r,a})^2}$, where $\epsilon^{r,a} = \epsilon \pm i\eta$, and η is a small energy relaxation rate that takes into account the damping of quasiparticle states due to inelastic processes inside the electrodes. This parameter can be estimated from the electron-phonon interaction to be a small fraction of Δ [24]. To determine the Keldysh Green functions appearing in the current and noise expression we first use their relation with the advanced and retarded functions $G^{a,r}$,

$$\hat{G}^{+,-}(t,t') = \left(\hat{1} + \hat{G}^r \otimes \hat{\Sigma}^r\right) \otimes \hat{g}^{+,-} \otimes \left(\hat{1} + \hat{\Sigma}^a \otimes \hat{G}^a\right), \tag{7}$$

where the $\otimes$ product stands for an integration over the common time variable. The self-energy in this problem is simply given by $\hat{\Sigma}^{r,a}_{LL} = \hat{\Sigma}^{r,a}_{RR} = 0$ and $\hat{\Sigma}^{r,a}_{LR} = (\hat{\Sigma}^{r,a}_{RL})^\dagger = \hat{v}(t)$. The unperturbed Green function $\hat{g}^{+,-}$ are given by $\hat{g}^{+,-}(\epsilon) = [\hat{g}^a(\epsilon) - \hat{g}^r(\epsilon)]\, f(\epsilon)$, where $f(\epsilon)$ is the Fermi function. Finally, the functions $G^{r,a}$ satisfy the Dyson equations

$$\hat{G}^{r,a}(t,t') = \hat{g}^{r,a} + \hat{g}^{r,a} \otimes \hat{\Sigma}^{r,a} \otimes \hat{G}^{r,a}. \tag{8}$$

In order to solve the above integral equations it is convenient to work in the energy space. Thus, we Fourier transform the Green functions with respect to the temporal arguments

$$\hat{G}(t,t') = \frac{1}{2\pi} \int d\epsilon \int d\epsilon'\ \mathrm{e}^{-i\epsilon t} \mathrm{e}^{i\epsilon' t'}\, \hat{G}(\epsilon,\epsilon'). \tag{9}$$

Due to the special time dependence of the coupling elements (see Eq. 6), every Green function admits a Fourier expansion of the form

$$\hat{G}(t,t') = \sum_n \mathrm{e}^{in\phi(t')/2} \int \frac{d\epsilon}{2\pi} \mathrm{e}^{-i\epsilon(t-t')} \hat{G}(\epsilon, \epsilon + neV), \tag{10}$$

which, in other words, means that $\hat{G}(\epsilon,\epsilon') = \sum_n \hat{G}(\epsilon, \epsilon + neV)\delta(\epsilon - \epsilon' + neV)$. Thus, the calculation of the different transport properties is reduced to the determination of the Fourier components $\hat{G}^{r,a}_{nm}(\epsilon) \equiv \hat{G}^{r,a}(\epsilon + neV, \epsilon + meV)$. Eq. 10 indicates that the different transport properties of this system should contain terms oscillating with all the harmonic of the Josephson frequency.

In particular, $S(\omega,t)=\sum_n S_n(\omega)\exp[in\phi(t)]$. At finite bias voltage, we shall concentrate ourselves in the dc part of the noise, i.e. S_0, which for simplicity will be denoted as $S(\omega)$. This noise component can be expressed in terms of the Fourier components of the Green functions as follows

$$\begin{aligned} S(\omega) &= \frac{2e^2}{h}\sum_{\pm\omega,n}\int d\epsilon\ \mathrm{Tr}\left\{\hat{\sigma}_z\hat{D}^{+,-}_{RL,0n}(\epsilon\pm\omega)\hat{\sigma}_z\hat{D}^{-,+}_{LR,n0}(\epsilon)- \right. \\ &\left. \hat{\sigma}_z\hat{D}^{+,-}_{RR,0n}(\epsilon\pm\omega)\hat{\sigma}_z\hat{D}^{-,+}_{RR,n0}(\epsilon)\right\}, \end{aligned} \tag{11}$$

where we have defined $\hat{D}(t,t')\equiv\hat{v}(t)\hat{G}(t,t')$ to simplify the notation. The last step in the calculation is the computation of the Fourier components $\hat{G}^{r,a}_{nm}$.. They can be determined by Fourier transforming Eq. 8 and using the relation of Eq. 10. Thus for instance, it can be shown that the components $\hat{G}^{r,a}_{RR,nm}\equiv\hat{G}_{nm}$ fulfill the following algebraic linear equation (assuming that the contact is symmetric)

$$\hat{G}_{nm}=\hat{g}_{nm}\delta_{n,m}+\hat{\mathcal{E}}_{nn}\hat{G}_{nm}+\hat{\mathcal{V}}_{n,n-2}\hat{G}_{n-2,m}+\hat{\mathcal{V}}_{n,n+2}\hat{G}_{n+2,m}, \tag{12}$$

where the matrix coefficients $\hat{\mathcal{E}}_{nn}$ and $\hat{\mathcal{V}}_{n,m}$ can be expressed in terms of the Green's functions of the uncoupled electrodes, as

$$\begin{aligned} \hat{\mathcal{E}}_n &= v^2\begin{pmatrix} g_ng_{n-1} & f_ng_{n+1} \\ f_ng_{n-1} & g_ng_{n+1}\end{pmatrix} \\ \hat{\mathcal{V}}_{n,n+2} &= -v^2f_{n+1}\begin{pmatrix} f_n & 0 \\ g_n & 0\end{pmatrix} \\ \hat{\mathcal{V}}_{n,n-2} &= -v^2f_{n-1}\begin{pmatrix} 0 & g_n \\ 0 & f_n\end{pmatrix}, \end{aligned} \tag{13}$$

In these equations the notation $g_n=g_i(\epsilon+neV)$ is used. Notice that this set of linear equations is analogous to those describing a tight-binding chain with nearest-neighbor hopping parameters $\hat{\mathcal{V}}_{n,n+2}$ and $\hat{\mathcal{V}}_{n,n-2}$. A solution can then be obtained by standard recursive techniques (see Ref. [9] for details), which permits to obtain analytical results in some limits, and in any case an efficient numerical evaluation of the Fourier components. In the case of zero bias, all the harmonics of noise give a finite contribution. In this limit the calculation can be greatly simplify noticing that the problem becomes stationary (the time-dependent Green functions only depend on the time difference) and using the equilibrium relations

$$\hat{G}^{+,-}(\epsilon) = \left[\hat{G}^a(\epsilon)-\hat{G}^r(\epsilon)\right]f(\epsilon), \tag{14}$$

$$\hat{G}^{-,+}(\epsilon) = \left[\hat{G}^a(\epsilon)-\hat{G}^r(\epsilon)\right]\left[f(\epsilon)-1\right]. \tag{15}$$

In this limit one can obtain analytical results, as we shall detail in the next section.

3. Theoretical results

3.1. THERMAL NOISE

In the limit of vanishing bias voltage the current is due to Cooper pair tunneling (non-dissipative Josephson current). One would naively expect that thermal noise at temperatures $k_BT \ll \Delta$ would be negligible. This is certainly the case for a tunnel junction with a exponentially small barrier transparency. However, in a superconducting point contact the situation can be radically different due to the presence of the Andreev states inside the gap. Fluctuations in the population of these states can lead to a huge increase of the noise in certain conditions. The noise spectral density in this regime was calculated in Ref. [11] using the formalism discussed in the previous section. The spectrum at subgap frequencies can be understood in terms of a simple two-level model describing the Andreev states. Let us recall that for a single channel contact of transmission τ there are two bound states at energies $\pm\epsilon_S$, where $\epsilon_S = \Delta\sqrt{1-\tau\sin^2\phi/2}$. The zero temperature supercurrent is just given by $I(\phi) = -(2e/\hbar)\partial_\phi\epsilon_S$. In such a two-level system at finite temperature the upper level can be thermally populated giving rise to a reverse in the sign of the supercurrent. It is important to notice that in a real system the Andreev bound states are affected by a long but finite life-time fixed by the typical inelastic tunneling rate of the system $\eta \ll \Delta$ [24]. The current fluctuations thus correspond to a type of telegraph noise in which the system switches between positive and negative current with a characteristic time given by $\hbar/\eta$ [10].

As the gap between the Andreev states decreases with increasing contact transmission one could expect a large increase of the noise. In fact, the results of Ref. [11] show that the noise exhibits a huge increase when $\Delta\sqrt{1-\tau} \ll k_BT$. The exact result for the zero-frequency noise is found to be given by

$$S(0,\phi) = \frac{2e^2}{h}\frac{\pi}{\eta}\frac{\Delta^4\tau^2\sin^2(\phi)}{\epsilon_S^2} f(\epsilon_S)\left[1-f(\epsilon_S)\right]. \qquad (16)$$

From this expression one can verify that the thermal noise approaches its maximum value, $e^2\Delta^2/\hbar\eta$, when $\phi \to \pi$ and $\tau \to 1$, for any finite temperature. This result is strictly valid in the limit of small inelastic tunneling rate, $\eta \ll \tau\Delta$, and in the low transmission regime differ strongly from the noise spectrum that is obtained for tunnel junctions using standard tunnel theory [25], which yields $S(0) \sim \tau(1+\cos\phi)\ln(\Delta/\eta)$. As shown in

[26], the reason for this discrepancy is that the limits $\tau \to 0$ and $\eta \to 0$ actually do not commute: when $\eta \ll \tau\Delta$ the main contribution to the noise comes from the MAR processes building up the Andreev states and should be taken into account up to infinite order; while for $\eta \gg \tau\Delta$ higher order MAR processes become heavily damped and the lowest order perturbation theory in the tunnel Hamiltonian gives the correct answer.

It is interesting to point out that the contact linear conductance, $G(\phi)$, can be obtain from Eq. (16) through the fluctuation dissipation theorem, which states that $S(0,\phi) = 4k_BTG(\phi)$. The expression of the linear conductance can also be obtained by a direct calculation of the current in the limit $V \to 0$ [26]. The full noise spectrum in the zero bias limit exhibits also an additional peak at $\omega = 2\epsilon_s$ associated with excitations from the lower to upper Andreev state. The weight of this peak is found to be given by [11]

$$S(2\epsilon_S) = \frac{2e^2}{h}\frac{\pi}{\eta}\frac{\Delta^4\tau^2(1-\tau)\sin^4(\phi)}{\epsilon_S^2}\left[f^2(\epsilon_S) + f^2(-\epsilon_S)\right] \qquad (17)$$

It is worth noticing that in the zero temperature limit this is the only remaining subgap feature in the noise spectrum. This expression clearly shows that $S(2\epsilon_S)$ is proportional to the square of the zero temperature supercurrent with a Fano reduction factor $(1-\tau)$.

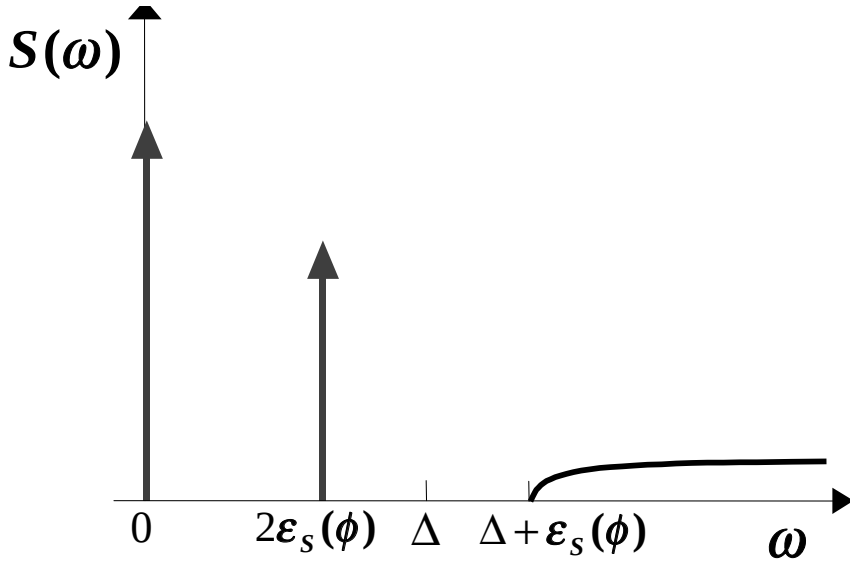

Figure 2. Schematic representation of the thermal noise spectrum. Notice the discrete character of the spectrum for $\omega < \epsilon_S + \Delta$. Only two sharp resonances (width $\sim \eta$) at $\omega = 0$ and $\omega = 2\epsilon_S$ appear due to the contribution of the subgap states.

In addition to the subgap features, the noise spectrum has a continuous part for $\omega > \epsilon_S + \Delta$. Figure 2 illustrates the overall features in the zero bias noise spectrum. Notice the small width of the subgap resonances which is controlled by the inelastic tunneling rate η.

3.2. SHOT NOISE

When a finite bias voltage is applied, the current is due to quasiparticle tunneling mediated by MAR processes. In this section we shall concentrate in the analysis of the shot noise regime ($eV \gg k_B T$). As discussed in the introduction, shot noise in the Poissonian limit provides a measure of the charge of the quasiparticles being transmitted. The question then arises on whether this relation still holds for superconducting junctions in the coherent MAR regime. As we discuss below, the situation is far more complex in this case. Only in the low transmission regime one can clearly identify the charge which is being transmitted for a given voltage bias.

In general, it is not possible to obtain a compact expression for the noise spectrum in the non-equilibrium situation. The zero-frequency noise for arbitrary transmission and voltage has been calculated in Refs. [12, 13]. The numerical results are summarized in Fig. 3, where we also show the dc current for comparison. As can be observed, the most prominent features in the shot noise are: (i) the presence of a strongly pronounced subgap ($V \leq 2\Delta$) structure, which remains up to transmissions close to one (in the dc current this structure is only pronounced for low transmissions). In the low transparency limit the shot noise subgap structure consists of a series of steps at voltages $eV_n = 2\Delta/n$ (n integer) as in the case of the dc current. (ii) The shot noise can be much large than the Poisson noise ($S_{Poisson} = 2eI$), as can be seen in Fig. 4. (iii) For higher transmissions there is a steep increase in the noise at low voltages. (iv) For perfect transmission the shot noise is greatly reduced. (v) In the large voltage limit ($eV \gg \Delta$) there is an excess noise with respect to the normal case.

The shot noise can be analyzed with more detail in the two opposite limits: $\tau \to 0$ (tunnel) and $\tau \to 1$ (ballistic regime). Let us start by considering the low transmission regime ($\tau \ll 1$). In this limit the electronic transport can be analyzed as a multiple sequential tunneling process in which the dc current can be written as the addition of the tunneling rates corresponding to different MAR processes: $I_0(V) = \sum_n ne\Gamma_n(V)$, with $\Gamma_n = (2/h)\int d\epsilon R_n(\epsilon)$, where the probability of an nth-order Andreev process R_n is given by [9]

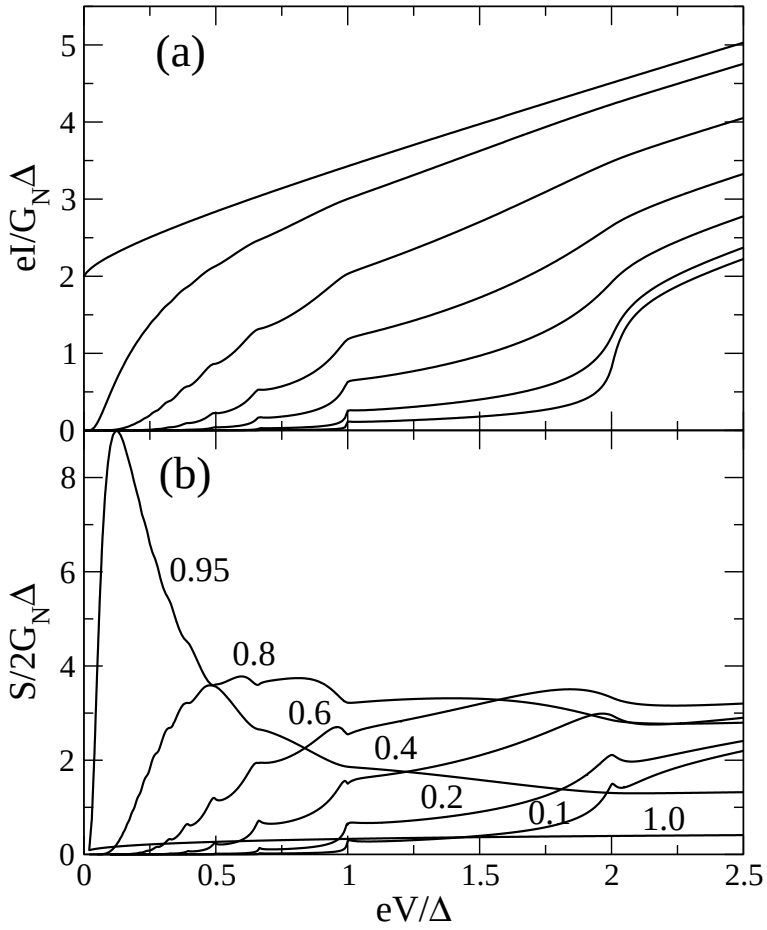

Figure 3. (a) Current-voltage and (b) noise-voltage characteristics for different transmissions at zero temperature. The values of the transmission are the same in both panels. $G_N = (2e^2/h)\tau$ is the normal conductance.

$$R_n(\epsilon) = \frac{\pi^2\tau^n}{4^{n-1}}\left[\prod_{k=1}^{n-1}|p(\epsilon - keV)|^2\right]\rho(\epsilon - neV)\rho(\epsilon)\ ;\text{where}\ \ \epsilon \in [\Delta, neV - \Delta], \tag{18}$$

where $\rho(\epsilon) = |\epsilon|/\sqrt{\epsilon^2 - \Delta^2}$ is the dimensionless BCS density of states and $p(\epsilon) = \Delta/\sqrt{\Delta^2 - \epsilon^2}$ is the Cooper pair creation amplitude. This expression for R_n clearly displays the different ingredients in a MAR processes, i.e. it is proportional to the initial and final density of states, to the probabitlity of creating $n-1$ Cooper pairs and to the probability of a quasiparticle crossing

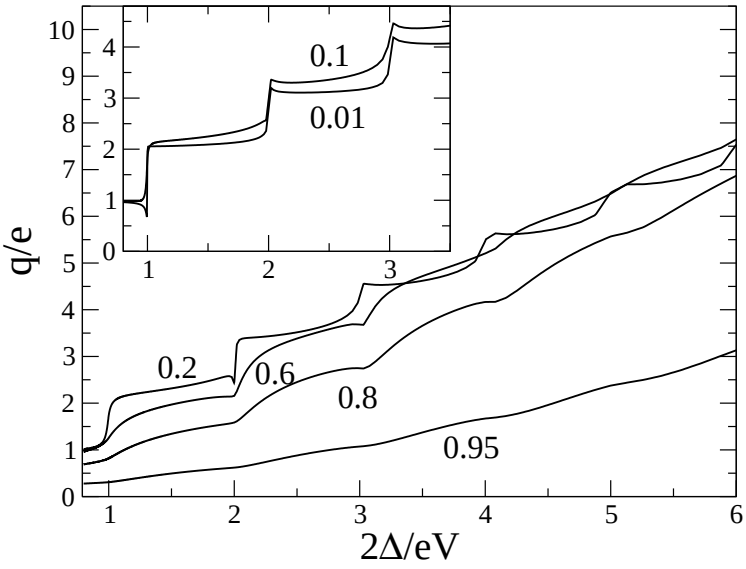

Figure 4. Effective charge $q = S/(2I)$ as a function of the reduced inverse voltage for different transmissions.

n times the interface (τ^n). This current expression already suggests that the transmitted charge associated with each MAR process is well defined in this limit. In contrast to a normal channel, characterized by a binomial distribution (the electron is either emitted or reflected), in the present case the quasiparticles can tunnel through many different channels (corresponding to the different MAR processes) giving rise to a multinomial distribution. Consequently, the shot noise can be written as

$$S(0,V) = \frac{4e^2}{h} \int d\epsilon \left[\sum_{n=1}^{\infty} n^2 R_n - \left(\sum_{n=1}^{\infty} n R_n \right)^2 \right]. \tag{19}$$

The MAR probability, R_n, is proportional to τ^n and is finite only for $eV > 2\Delta/n$. Therefore, when $\tau \to 0$ in the voltage interval $[2\Delta/en, 2\Delta/e(n-1)]$ the main contribution to the current comes from a n-order MAR, and the current distribution becomes Poissonian with a different charge depending on the voltage range. In fact, the effective charge defined as $q = S(0,V)/2I$ exhibits in this limit a staircase behavior given by $q(V)/e = \mathrm{Int}[1+2\Delta/eV]$. In Fig. 4 we show the effective charge calculated for different transmissions. As can be observed $q(V)$ increases for decreasing bias as $1/V$, its shape becoming progressively steplike for decreasing transmission.

In the ballistic regime the calculation of the amplitudes for the MAR processes is simplified due to the absence of interference effects due to backscattering. Averin and Imam [10] derived the following expression for the spectral density in this limit

$$\begin{aligned} S(\omega,V) &= \frac{4e^2}{h}\sum_{\pm\omega}\int d\epsilon\, F(\epsilon)\left[1-F(\epsilon\pm\hbar\omega)\right] \\ &\times\left[1+2\,\mathrm{Re}\sum_{k=1}^{\infty}\prod_{l=1}^{k}a(\epsilon+leV)a^*(\epsilon+leV\pm\hbar\omega)\right]. \end{aligned} \tag{20}$$

Here $a(\epsilon)=(\epsilon+i\sqrt{\Delta^2-\epsilon^2})/\Delta$ is the amplitude of Andreev reflection from the superconductors, and F is the nonequilibrium distribution of quasiparticles in the point contact,

$$F(\epsilon)=f(\epsilon)+\sum_{n=0}^{\infty}\prod_{m=0}^{n}|a(\epsilon-meV)|^2\left[f(\epsilon-(n+1)eV)-f(\epsilon-neV)\right]. \tag{21}$$

At zero frequency and zero temperature, this expression gives rise to the rather featureless curve as a function of bias shown in Fig. 3 for $\tau=1$. The great reduction of the noise is due to the fact the probabilities of the different MARs are equal to 1 inside the gap. However, the noise does not vanish completely, like in the normal case, because the MAR probabilities are less than 1 outside the gap. As mentioned above, an interesting feature of the noise is the huge enhancement close to perfect transparency at small voltages (see curve $\tau=0.95$ in Fig. 3). Following the analysis of Naveh and Averin [13], the behavior of the noise in this limit can be understood in terms of Landau-Zener transitions between the two ballistic subgap states. Within this picture the noise is originated by the stochastic quantum-mechanical nature of the transitions between the two states. As explained in the previous section, these two states carry the currents $\pm(e\Delta/\hbar)\sin\phi/2$, where ϕ is the Josephson phase difference across the junction, with $\dot{\phi}=2eV/\hbar$. In each period of the Josephson oscillations the junction either stays on one of the Andreev levels and carries the current of the same sign during the whole oscillation period, or either makes a transition between the two states at $\phi=\pi$ so that the current changes sign for the second half of the period. The first case occurs with probability $p=\exp\{-\pi R\Delta/eV\}$, where $R=1-\tau$, and then the charge

$$Q_0=\frac{e\Delta}{\hbar}\int_0^{T_0}dt\sin\phi/2=\frac{2\Delta}{V},$$

where $T_0=\pi\hbar/eV$ is the period of the Josephson oscillations, is transferred through the junction. In the second case the probability is $1-p$ and no net

charge is transferred. Therefore statistics of charge Q transferred through the junction during the large time interval $T \gg T_0$ is characterized by a binomial distribution with probability p. The noise is then given by

$$S(0,V) = \frac{2(\langle Q^2\rangle - \langle Q\rangle^2)}{T} = \frac{8e\Delta^2}{\pi\hbar V} p(1-p)\,. \tag{22}$$

The noise reaches a maximum at small voltages $eV \simeq \pi R\Delta$ and its peak value increases with decreasing R as $1/R$. One can check that Eq. (22) describes accurately the low-voltage behavior of the curves with small R in Fig. 3. It is also interesting to analyze the large voltage limit, in which the zero-frequency noise behaves as $S(eV \gg \Delta = (4e^2/h)\tau(1-\tau)V + S_{exc}$, i.e. the shot-noise of a normal contact with transmission τ plus a voltage-independent "excess noise" S_{exc}. The excess noise as a function of transmission is shown in Fig. 5. S_{exc} has the same physical origin as the excess current (I_{exc}), which arises from the contribution of the first order Andreev process. We obtain that at zero temperature S_{exc} is twice the excess noise of a N-S contact [27] with the same transmission. In particular, this relation yields $S_{exc} = 2/5eI_{exc}$ for the perfect ballistic case [28].

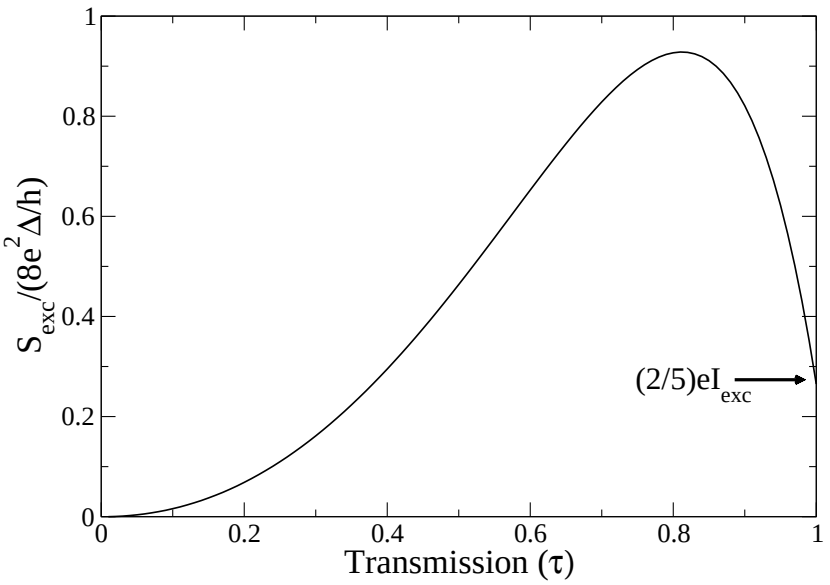

Figure 5. Excess noise as a function of the transmission at zero temperature.

3.3. NON-EQUILIBRIUM NOISE AT FINITE FREQUENCIES

Our knowledge about shot noise in the coherent MAR regime is mainly restricted to the zero frequency limit. However, a rich frequency-dependency is to be expected according to the strong non-linear behavior of the IV characteristics. This dependency should contain very valuable information on the dynamics of quasiparticles in the MAR regime. Additonal interest on the full noise spectrum arises from its connection with the Coulomb blockade phenomena as recently pointed out in Ref. [29]. In this work it was shown that the deviation from the Ohmic behavior of normal a coherent conductor due to its electromagnetic environment can be expressed in terms of the conductor noise spectrum $S(\omega, V)$. Thus, the dynamical Coulomb blockade in a circuit containing a quantum point contact should vanish in the same way as shot noise when the contact transmissions approach unity. It is to be expected that a similar relation should hold in the superconducting case. In order to get an idea about the behavior of the full noise spectrum we have extended the calculations of the previous section to the finite-frequency domain. In Fig. 6 we show some numerical results for the finite-frequency shot noise for different transmissions. The most important feature is the splitting of the subharmonic gap structure, which now takes place at voltages $eV = (2\Delta \pm \hbar\omega)/n$, with n integer. This is specially clear at low transparencies and at frequencies $\hbar\omega < \Delta$ (see Fig. 6(a)). This result can be understood with the sequential analysis described in the previous section. As in the case of the zero-frequency noise, the subharmonic gap structure is progressively washed out as the transparency is increased. Close to perfect transparency the main feature is the suppression of the peak at low voltages. When $\tau = 1$ the noise spectrum is almost featureless and exhibits a linear increase with frequency. The consequences of these findings on the dynamical Coulomb blockade of multiple Andreev reflections is currently under investigation.

4. Experimental studies of noise in SNS nanostructures

Motivated by some of the previously discussed theoretical predictions, shot noise has been studied experimentally in different types of SNS nanostructures. In 1997, Dieleman et al. observed what seemed to be a divergence of the effective charge at low voltages in NbN/MgO/NbN tunnel junctions [30]. The measured junctions consisted probably of parallel SNS point contacts due to the presence of small deffects acting as "pin-holes" in the tunnel barrier. This interpretation was confirmed by the observation of a finite subgap current exhibiting the typical structure at $eV = 2\Delta/n$. The mean transmission of the pin-holes was estimated to be $\tau \simeq 0.17$. In spite of the rather large error bars in the noise determination it was possible to observe

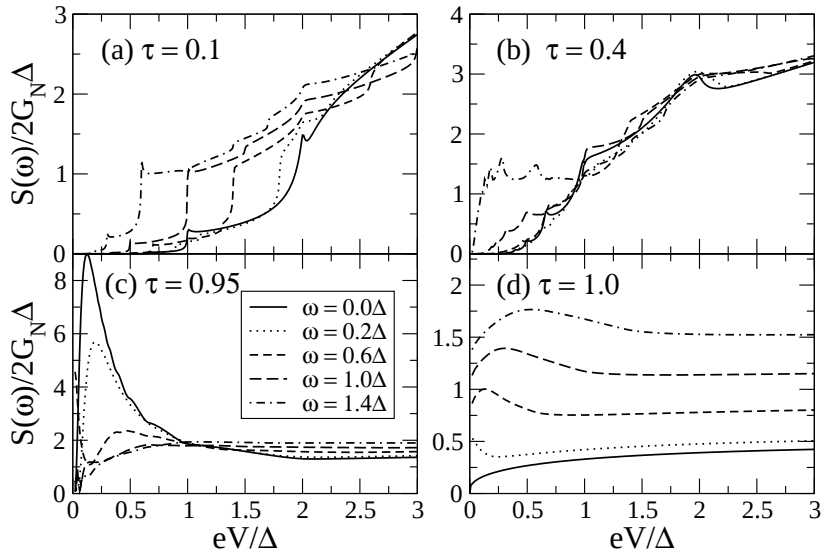

Figure 6. Finite frequency shot noise as a function of the voltage for different transmission and frequencies at zero temperature.

a clear increase of the effective charge with decreasing voltage. Dieleman et al. developed a qualitative explanation of their data within the framework of the semiclassical theory of MAR of Refs. [5]. The increase of the effective charge at low voltages has also been observed in diffusive SNS junctions by Hoss et al. [31]. They used high transparency Nb/Au/Nb, Al/Au/Al and Al/Cu/Al junctions prepared by lithographic techniques. Although being diffusive, the normal region is these junctions was smaller than the phase coherence lenght, which allowed to observe the coherent MAR regime. On the other hand, the junctions presented a very small critical current, which permitted to reach the low voltage regime. The excess noise in these experiments exhibited a pronounced peak at very low voltages (of the order of a few μV) corresponding to an effective charge increasing much faster than the predicted $1/V$ behavior. It should be pointed out that there is at present no clear theory for diffusive SNS junctions in the coherent MAR regime.

4.1. MEASUREMENTS OF SHOT NOISE IN WELL CHARACTERIZED ATOMIC CONTACTS

As we emphasized in the introduction, atomic-size contacts provide an almost ideal "test-bed" for many of the predictions of the theory. Since all

their characterstic dimensions are of the order of the Fermi wavelenght, atomic contacts are perfect quantum conductors, even at room temperature, and accomodate only a small number of conduction channels. For one-atom contacts the number of conduction channels is directly related to the number of valence orbitals of the central atom [18]. For example gold one-atom contacts contain only one channel, while aluminum and lead have three, and niobium five. For such a small number of channels it is possible to determine with good accuracy the mesoscopic code [17] from the precise measurement of the current-voltage characteristic in the superconducting state. The discovery that their mesoscopic "PIN-code", i.e. the set of transmission eigenvalues $\{\tau_n\}$, could be accurately decoded, paved a way to a new generation of quantum transport experiments in which the measured quantities could be compared to the theoretical predictions without adjustable parameters.

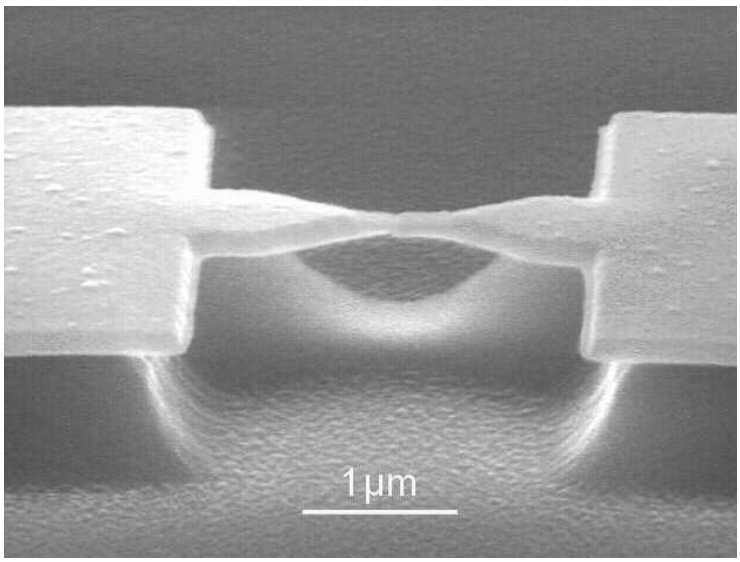

Figure 7. Micrograph of a nanofabricated break junction used in the noise measurements of Ref. [21].

It is worth mentionning that van den Brom and van Ruitenbeek [32], reversing this point of view, have performed shot noise measurements in atomic-size contacts in the normal state, in order to get information about the number of conduction channels and their transmission probabilities(see article by JVR in this book). For 27 different gold contacts they measured a spectral density well below the poissonian value, indicating that current

is mostly carried by well transmitting channels. The values of the conductance and the shot noise density are related respectively to the first and second moment of the transmission probability distribution. Because from two parameters the code can be disentangled only if the contact contains no more than two conduction channels, their results were quantitative only for total conductances below two conductance quanta. For a single gold atom contact the conductance is about one and their shot noise measurements established that the contribution of partially transmitted conduction channels is only a few percent.

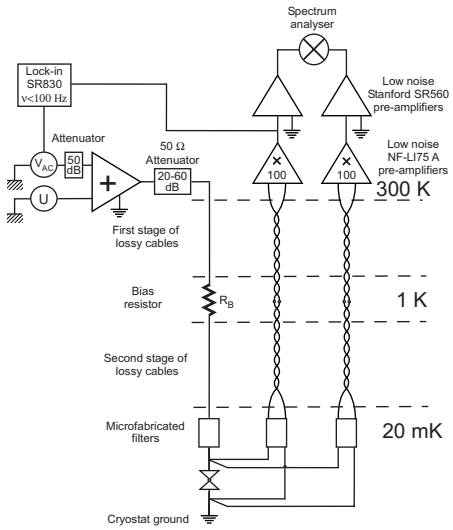

Figure 8. Schematic representation of the measurement set-up consisting of a coaxial line to bias the atomic-size contact (two triangle symbol) and of two twisted-pair lines used to measure twice the voltage across it. The spectrum analyzer calculates the cross-correlation of these two signals.

In a recent work, we have used nanofabricated Al break junctions for analyzing shot noise in atomic-size contacts. A micrograph of a nanofabricated junction is shown in Fig. 7. It consists of a metallic bridge clamped to an elastic substrate and suspended over a few micrometers between two

anchors. The bridge presents in its center a constriction with a diameter of approximately 100 nm. In order to obtain an atomic-size contact, the substrate is first bent till the bridge breaks at the constriction. The two resulting electrodes are then slowly brought back into contact. The high mechanical reduction ratio of the bending bench allows to control the number of atoms forming the contact one by one; in this way, single atom contacts can be produced in a controlled fashion. Nanofabricated atomic-size contacts are extremely stable and can be maintained for days. Due to its high mechanical stability, this technique [33] is particularly suitable for shot-noise measurements at very low bias currents.

The set-up used to measure shot noise is depicted in Fig 8. It consists basically of one coaxial line, used to bias the on-chip grounded atomic contact, and of two twisted-pair lines used to obtain two independent measurements of the voltage across with two sets of low-noise amplifiers. With this set-up current fluctuations are thus not directly measured, but instead inferred from the fluctuations of the voltage across the contact. The current and voltage fluctuations spectral densities S_I and S_V respectively, are related, at a given voltage V through $S_V(V) = R_D^2 S_I(V)$, where $R_D(V) = \partial V/\partial I(V)$ is the differential resistance. In the normal state, this differential resistance is essentially constant in the voltage range in which the experiments are carried out, and equals R_N, the normal resistance of the contact. In the superconducting state, the differential resistance can be highly non-linear and is determined using a lock-in amplifier for each point at which the noise is measured.

All noise sources along the measurement lines, like the Johnson-Nyquist thermal noise of the resistors or the current and voltage noise of the amplifiers input stages, induce fluctuations that poison the shot noise signal. Because of that, the measurement lines and the bias line were carefully designed and built so as to limit and keep under control this additional noise. As mentionned before, the voltage across the atomic-size contact is measured twice and the real part of the cross-correlation spectrum of the two amplified signals is calculated in real time by a spectrum analyzer. This cross-correlation technique allows one to get rid of the voltage noise coming from the preamplifiers and the measurement lines that poison the white noise signal. Typically, the spectra were measured over 800 points in a frequency window $[360, 3560Hz]$ and averaged 1000 times in 4 min (a detailed discussion of the setup calibration can be found in [34]). Once the PIN-code of a given contact has been determined, a first check of consistency is obtained from the measurement of the current fluctuations in the normal state. The normal state is recovered without changing the temperature by applying a small magnetic field (of the order of 50 mT) which does not affect the transmissions. The measured low frequency spectral density

as a function of the average current is shown in Fig. 9 for different contacts. These results can be compared with the predictions of the theory for noise in normal contacts [27]

$$S_I(V,T,\{\tau_i\}) = 2eV\coth(\frac{eV}{2k_BT})G_0\sum_i \tau_i(1-\tau_i) \qquad (23)$$
$$+4k_BTG_0\sum_i \tau_i^2 \ .$$

The full lines in Fig. 9 corresponds to Eq. (23) using the set of PIN-codes extracted from the analysis of the superconducting IV curves. As can be observed, there is a remarkable agreement between theoretical and experimental results. It should be emphasized that there are no fitting parameters in this comparison as the transmission coefficients have been determined independently. This good agreement provides additional proof of the accuracy that can be obtained in the determination of the contact PIN-code.

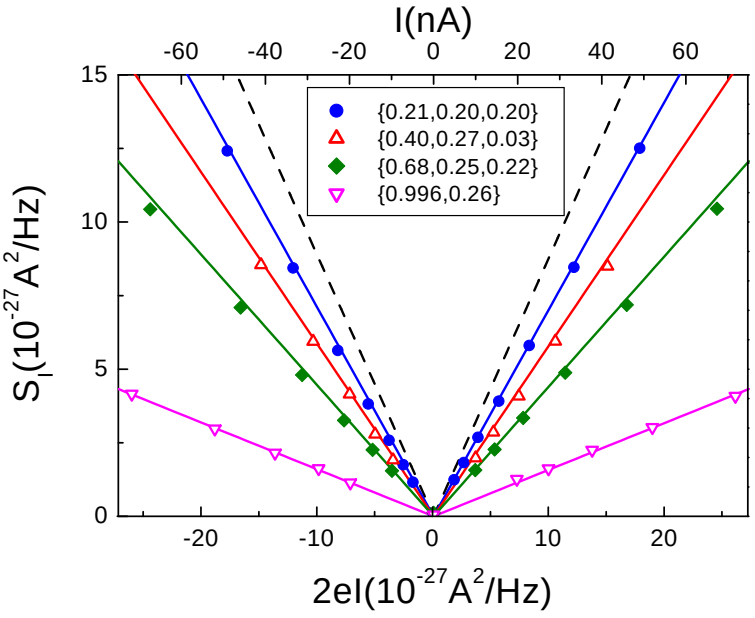

Figure 9. Symbols: measured low frequency spectral density of aluminum atomic-size contacts versus poissonian spectral density $2eI$. Solid lines are prediction of for the corresponding mesoscopic codes. The dashed line is the poissonian limit.

The following step in the experiments was the measurement of the noise in the superconducting state. Fig. 10 shows the measured spectral densities as a function of bias voltage for three different contacts. In contrast to the behavior in the normal case, the measured S_I is markedly nonlinear and for high enough voltages it is above the value determined in the normal state. For comparison, the theoretical predictions for the corresponding PIN-codes are shown as full lines. As can be observed the agreement between theory and experiment is quantitative both regarding the subgap structure and the excess noise at large bias. The data can be presented in a more intu-

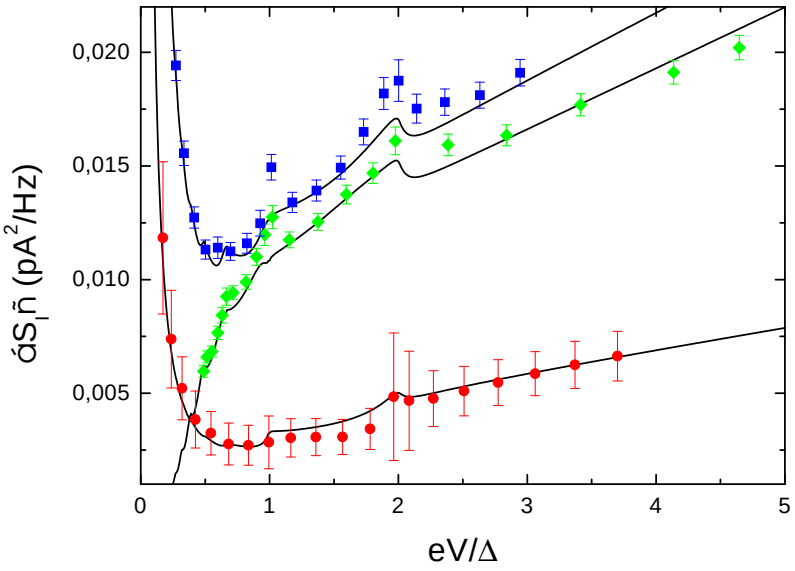

Figure 10. Dots: Measured current fluctuation spectral density as a function of reduced voltage of three atomic-size contacts. Mesoscopic PIN codes: $\{0.98, 0.55, 0.24, 0.22\}$ (squares), $\{0.68, 0.25, 0.22\}$ (diamonds), $\{0.996, 0.26\}$ (circles). Full curves: theoretical predictions of the MAR theory using the mesoscopic code.

itive way, by plotting the effective charge $q = S_I/2I$ as a function of the inverse voltage. Fig. 11 shows the data for a contact having an intermediate transmission. Let us recall that only in the tunnel limit the theory predicts that q should increase in a perfect staircase pattern with decreasing bias. Our setup sensitivity was not enough to measure the noise in this limit of very small bias currents. However, the emergence of a staircase pattern can already be recognized in the data shown in Fig 11.

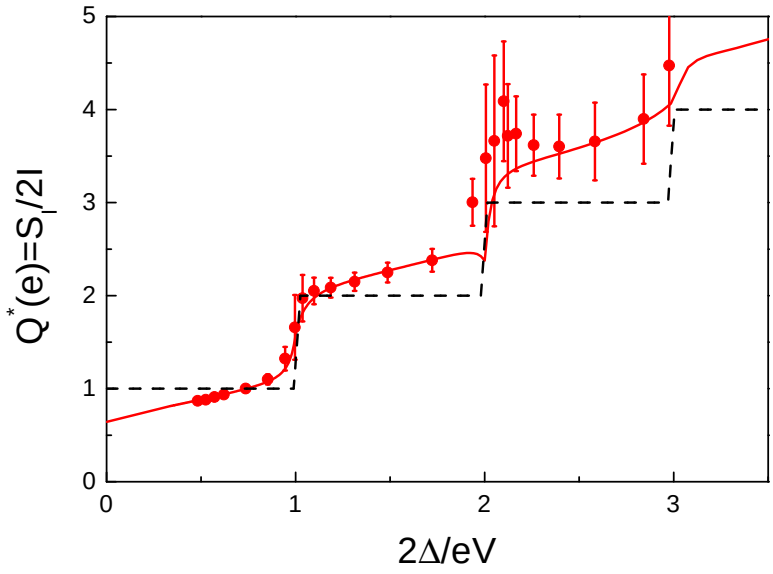

Figure 11. Effective size of the shot-noise "pellets", in units of e, as a function of the inverse reduced voltage for a contact in the superconducting state. Dashed line : MAR theory prediction in the tunnel limit. As the voltage increases, MAR processes of lower order set-in one by one leading to this perfect staircase pattern. Dots : Data for an aluminum atomic contact with mesoscopic PIN code $\{0.40, 0.27, 0.03\}$. Full line : MAR theory prediction for this code.

5. Conclusions

We have analyzed several aspects of noise phenomena in superconducting quantum point contacts. The more remarkable features both in the equilibrium and non-equilibrium current fluctuations appear as a consequence of the underlying MAR mechanism for electronic transport. At zero bias voltage huge supercurrent fluctuations are predicted due to transitions between the subgap Andreev states. At finite bias the noise spectrum exhibits a very pronounced subgap structure which corresponds to the onset of higer order MAR processes when the voltage is reduced. The effective charge generally increase as $1/V$ but is only quantized in the tunnel limit when the interference between different MAR processes can be neglected. All these properties exhibit a highly non-trivial dependence on the contact transparency. On the experimental side, noise measurements in well characterized superconducting atomic contacts have provided an unambiguous test of the theoretical

predictions. The possibility of obtaining the corresponding set of transmissions (the PIN-code) from the analysis of the subgap structure in the superconducting IV curves has allowed a direct comparison with theory without fitting parameters. The quantitative agreement found for the noise completes a comprehensive series of tests which includes the measurement of the supercurrent [20] and the current-voltage characteristics [**?**]. Finally, the study of non-equilibrium noise in the finite-frequency domain appears as a very promising avenue of reaserch.

* Present address: Institut für Theoretische Festkörperphysik, Universität Karlsruhe, 76128 Karlsruhe, Germany

References

1. Ya.M. Blanter and M. Büttiker, Phys. Rep. **336**, 1 (2000).
2. W. Schottky, Ann. Phys. (Leipzig) **57**, 541 (1918).
3. L. Saminadayar, D.C. Glattli, Y. Lin and B. Etienne, Phys. Rev. Lett. **79**, 2526 (1997); R. de-Picciotto, M. Reznikov, M. Heiblum, V. Umansky, G. Bunin and D. Mahalu, Nature **389**, 162 (1997); M. Reznikov *et al.*, Nature **399**, 238 (1999).
4. X. Jehl *et al.*, Nature **405**, 50 (2000).
5. T.M. Klapwijk, G.E. Blonder and M. Tinkham, Physica B **109&110**, 1657 (1982); M. Octavio, G.E. Blonder, M. Tinkham, and T.M. Klapwijk, Phys. Rev. B **27**, 6739 (1983).
6. G.B. Arnold, J. Low Temp. Phys. **68**, 1 (1987).
7. E.N. Bratus, V.S. Shumeiko, and G. Wendin, Phys. Rev. Lett. **74**, 2110 (1995).
8. D. Averin and A. Bardas, Phys. Rev. Lett. **75**, 1831 (1995).
9. J.C. Cuevas, A. Martín-Rodero and A. Levy Yeyati, Phys. Rev. B **54**, 7366 (1996).
10. D.V. Averin and H.T. Imam, Phys. Rev. Lett. **76**, 3814, (1996).
11. A. Martín-Rodero, A. Levy Yeyati and F.J. García-Vidal, Phys. Rev. B, **53**, 8891 (1996).
12. J.C. Cuevas, A. Martín-Rodero and A. Levy Yeyati, Phys. Rev. Lett. **82**, 4086 (1999).
13. Y. Naveh and D.V. Averin, Phys. Rev. Lett. **82**, 4090 (1999).
14. C.J. Muller, J.M. van Ruitenbeek and L.J. de Jongh, Physica C **191**, 485 (1992).
15. N. van der Post, E.T. Peters, I.K. Yanson, and J.M. van Ruitenbeek, Phys. Rev. Lett. **73**, 2611 (1994).
16. M.C. Koops, G.V. van Duyneveldt, and R. de Bruyn Ouboter, Phys. Rev. Lett. **77**, 2542 (1996).
17. E. Scheer, P. Joyez, D. Esteve, C. Urbina and M.H. Devoret, Phys. Rev. Lett. **78**, 3535 (1997).
18. E. Scheer, N. Agraït, J.C. Cuevas, A. Levy Yeyati, B. Ludoph, A. Martín-Rodero, G. Rubio, J.M. van Ruitenbeek and C. Urbina, Nature **394**, 154 (1998).
19. B. Ludoph *et al.*, Phys. Rev. B **61**, 8561 (2000).
20. M.F. Goffman *et al.*, Phys. Rev. Lett. **85**, 170 (2000).
21. R. Cron *et al.*, Phys. Rev. Lett. **86**, 4104 (2001).
22. J.R. Schrieffer and J.W. Wilkins, Phys. Rev. Lett. **10**, 17 (1963).
23. L.V. Keldysh, Sov. Phys. JETP **20**, 1018 (1965).
24. S.B. Kaplan *et al.*, Phys. Rev. B **14**, 4854 (1976).
25. D. Rogovin and D.J. Scalapino, Annals of Physics **86**, 1 (1974).
26. A. Martín-Rodero, A. Levy Yeyati, and J.C. Cuevas, Physica B **218**, 126 (1996); A. Levy Yeyati, A. Martín-Rodero, and J.C. Cuevas, J. Phys.: Condens. Matter **8**, 449 (1996).

27. V.A. Khlus, Sov. Phys. JETP **66**, 1243 (1987).
28. J.P. Hessling, V.S. Shumeiko, Yu. M. Galperin and G. Wendin, Europhys. Lett. **34**, 49 (1996).
29. A. Levy Yeyati, A. Martín-Rodero, D. Esteve, and C. Urbina, Phys. Rev. Lett. **87**, 046802 (2001).
30. P. Dieleman *et al.*, Phys. Rev. Lett. **79**, 3486 (1997).
31. T. Hoss *et al.*, Phys. Rev. B **62**, 4079 (2000).
32. H.E. van den Brom and J.M. van Ruitenbeek, Phys. Rev. Lett. 82, 1526 (1999).
33. J.M. van Ruitenbeek, A. Alvarez, I. Piñeyro, C. Grahmann, P. Joyez, M.H. Devoret, D. Esteve, and C. Urbina, Rev. Sci. Instrum. 67, 108 (1996).
34. Ronald Cron, PhD dissertation, Université de Paris, that can be downloaded from http://www-drecam.cea.fr/drecam/spec/Pres/Quantro/Qsite/index.htm